UNIVERSIDAD DE SONORA
División de Ciencias Exactas y Naturales
Departmento de Investigación en Física

Study of the production of Higgs plus single top using events with a same sign dimuon pair in the final state at the Large Hadron Collider

BY:

Hiram Ernesto Damián

A thesis submitted in partial fulfillment of the requirements for the degree of:
Master of Science in Physics

Director:
Dr. José Feliciano Benítez Rubio

Hermosillo, Sonora November, 2019

I would like to dedicate this thesis to my loving mother...

Acknowledgements

I would like to acknowledge Dr. José Feliciano Benítez Rubio for his contributions and advises in order to develop and write this thesis. Also thank Dr. Javier Murillo and Dr. Cristina Oropeza for their observations and advises in my formation. Dr. Susana Alvárez for supporting during the process of the thesis. Acknowledgments to CONACYT for supporting this thesis with financial aid.

Resumen

Se presenta un estudio sobre la producción del boson de Higgs y un top quark (tH) en el canal de 2 muones con el mismo signo $\mu^{\pm}\mu^{\pm}$ usando datos publicados por el experimento CMS en el CERN. Estudiando este proceso se explora este mecanismo de producción del boson de Higgs que aún no se ha detectado experimentalmente. La sensibilidad esperada es calculada usando datos de tipo Asimov para 35.9 fb^{-1} de colisiones de protón-protón y es extrapolada la fase de alta luminosidad del LHC (HL-LHC). La sensibilidad de la señal es también estudiada para el modelo con acoplamiento de Yukawa invertido k_t=-1, donde k_t es el modificador del parámetro de acoplamiento de top-Higgs, en comparación con el Modelo Estándar. Para el modelo SM, se obtuvo un límite de 17 en la fuerza de la señal a un nivel de confianza de 95% con respecto al valor esperado usando 35.9 fb^{-1} de luminosidad integrada, mientras que con 3000 fb^{-1} se obtiene un límite de 4.3. Para el modelo modificado con k_t=-1, se obtiene un límite de 2.3 usando 35.9 fb^{-1} , mientras que con 3000 fb^{-1} se podría medir la fuerza de una posible señal con 10% de incertidumbre.

Abstract

We present a study on the production of a Higgs boson plus a single top quark (tH) in same sign dimuon channel $\mu^{\pm}\mu^{\pm}$ using data published by the CMS experiment at CERN. By studying this process, we explore a Higgs production mechanism which has not yet been observed experimentally. The expected sensitivity is estimated by using an Asimov dataset for 35.9 fb^{-1} of proton-proton collisions and is extrapolated to the high luminosity phase of the LHC (HL-LHC). The sensitivity is also studied for the model with inverted Yukawa coupling k_t=-1, where k_t is the top-Higgs coupling parameter modifier, for comparison with the Standard Model. For the SM, we obtained an upper limit of 17 on the signal strength with a confidence level of 95% with respect to the expected value using an integrated luminosity of 35.9 fb^{-1}, while with 3000 fb^{-1} we obtained an upper limit of 4.3. In the modified model with k_t=-1, we obtained an upper limit of 2.3 using 35.9 fb^{-1}, while in the 3000 fb^{-1} case a possible signal could be measured with an uncertainty of 10%.

Table of contents

List of figures

List of tables

Chapter 1

Introduction

1.1 General objective and motivations

Particle physics is a field of physics that studies the particles that create matter and their interactions to very small scale, even smaller than atoms. Particle physics studies the fundamental building blocks of matter (fermions) and their interactions via force carriers (bosons). All those particles and their properties are grouped in a theory called the Standard Model (SM). SM is a theory that describes the fundamental forces (except gravity) and classifies the elementary particles in bosons (integer spin) and fermions (half spin). The SM, created almost 50 years ago, has been the most successful theory in explaining the phenomena in the subatomic world.

One of the particles of the SM, the Higgs Boson, was recently discovered in 2012 in the ATLAS and CMS experiments at CERN. The discovery of Higgs boson in proton proton (pp) collisions marked a new era in particle physics due to its characteristic of giving matter the property of mass, according to previous theories and predictions. Since then, people around the world are working in the Large Hadron Collider (LHC) at CERN in order to detect the Higgs bosons in higher energies and different Higgs production processes. Also the Higgs boson is also important in cosmology, where theoretical investigations relate the Higgs boson to the cosmic inflation.

In recent years, there have been many studies of Higgs production processes at CERN in pp collisions, such as gluon fusion (ggF), VBF, WH, ZH and $t\bar{t}H$. In this work, we will analyze the production of a Higgs boson in association with a single top quark (tH) in pp collisions with the CMS experiment of the LHC.

The motivation of the work is that this production mechanism of the Higgs boson has not been observed before by any experiment. The exploration of Higgs production on the tH channel is a relatively new subject. Many channels are yet out of reach experimentally.

At the same time, many theoretical proposals are yet to be put to test. It is possible that studies on the Higgs boson give evidence of small deviations from the SM and test new physics that are beyond SM such as String Theory and Super-symmetry.

1.2 The Standard Model

The SM, created in the decade of the seventies, is a successful theory that explains the structure of matter and the interactions of three of the four fundamental forces which are electromagnetic, strong and weak. The gravitational force is yet to be included due to the scale of the interaction with respect to the other 3. All matter is composed of three kinds of particles: leptons, quarks and bosons, also called mediators.

For the leptons we have electrons (e), muons (μ), and taus (τ) with charge -1 and their neutrinos ν_e, ν_μ, ν_τ, are chargeless particles. All of them have a spin (intrinsic angular momentum) of $\frac{1}{2}$[1]. Quarks combine to form composite particles called hadrons. Quarks cannot be found in isolation, they always exist in form of hadrons that can be mesons or baryons. Mesons are made up of a quark-antiquark pair, such as pion (π) and kaon (K). Mesons were theorized by Yukawa in 1937 and discovered in 1947 by Powell[1]. Baryons are made of 3 quarks. Examples of baryons are protons and neutrons. Both types of particles can interact via the strong force. Since quarks and gluons only exist in bound, it is impossible to observe isolated quarks except the top quark, which decays before it has time to form a bound state [2].

Quarks were first theorized by Murray Gell-Mann and George Zweig in 1964. They were introduced as parts of an ordering scheme for hadrons, and there was little evidence for their physical existence until fixed target scattering experiments were conducted at the Stanford Linear Accelerator Center in 1968[1]. There are 6 of them: up (1968), down (1968), strange (1968), charm (theorized in 1970, discovered 1974), bottom (theorized 1973, discovered 1977), top (theorized 1973, discovered 1995).

Quarks have characteristics such as electric charge, mass, color charge, and spin. The quarks up, charm and top have in common a charge of $\frac{2}{3}$, while the down, strange and bottom quarks have charge of $-\frac{1}{3}$. Among them, the top quark is the most massive of all, while the up and down are the least massive. Some of the particles in the SM are not stable, so they decays and form particles with lower masses. Other particles do not decay or their lifetimes are very long. All the particles in the SM are shown in the Figure 1.1.

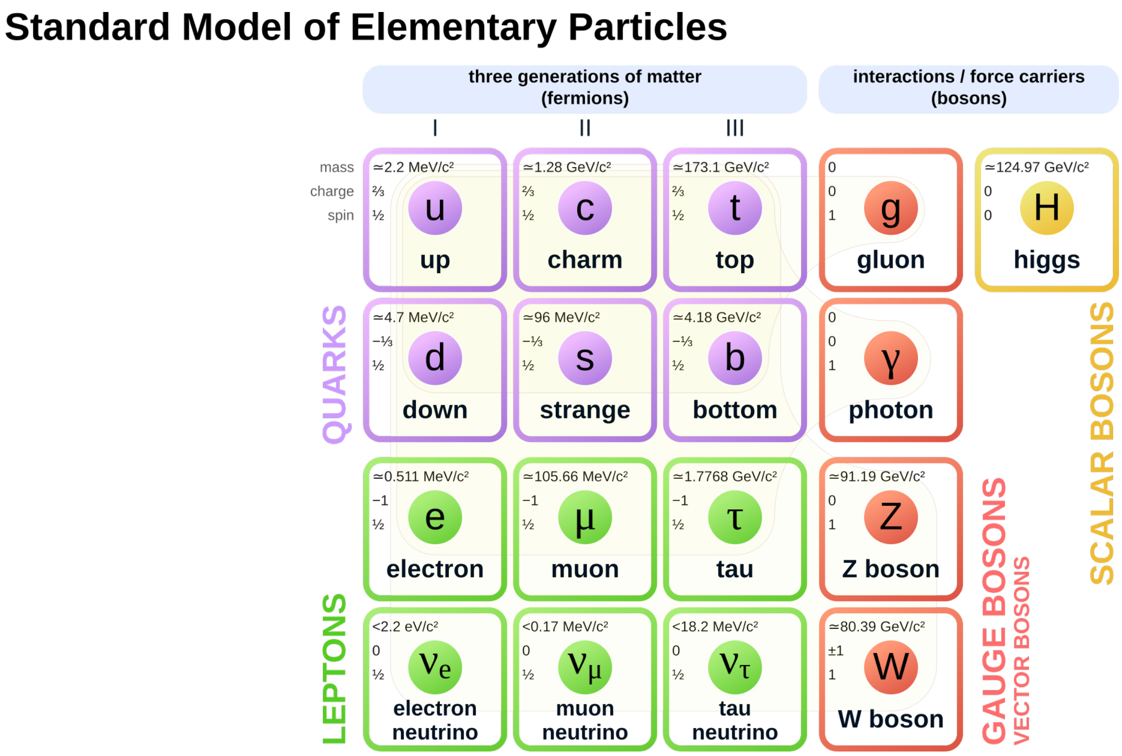

Fig. 1.1 List of particles in the Standard Model and their properties[3]

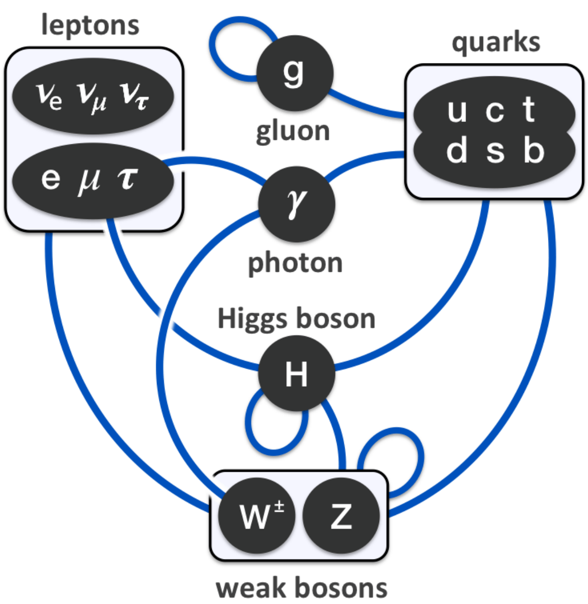

Fig. 1.2 Particle interactions in Standard model[4]

The last group of the family are the bosons, which have either spin 1 or 0. There are 5 bosons: $W^{\pm}$, Z with neutral charge are responsible for weak force; photon, a massless particle, is responsible for the electromagnetic force; gluons which are also massless, is related to the strong force and Higgs boson, recently discovered, is in charge of giving the property of mass to particles via the Higgs mechanism. Bosons let other particles interact, even themselves, which is shown in Figure 1.2. The W,Z and Higgs bosons, can interact with the most of the particles, while the gluons can only interact with quarks and with itself.

Table 1.1 contains the characteristics of each particle in the SM. The second column shows the masses of the particles, where the most massive particle is the top quark with 173 GeV. There are particles with mass equal to zero, such as the gluons, photons and the neutrinos. The third column corresponds to the charge of the particles. For the quarks, there are two different charges: $\frac{2}{3}$ for u,c and t and $-\frac{1}{3}$ for d,s and b. For the leptons, the charge is negative, except for neutrinos, which charge is zero. The bosons have a integer charge; ± 1 for W and 0 for Z, γ, H and g. The next column is the spin, where for fermions (quarks and leptons) is $\frac{1}{2}$ and for bosons is 1[1]. The Higgs boson is the only boson with spin 0. The next one is the lifetime of the particle, where it shows how long the particles exist before decay. Stable lifetime means that the particles do not decay or lifetime almost infinite. The last column is the distance of particles moving with speeds near light speed. This column illustrates the distance traveled in the predicted lifetime of the particle. And also give us a perspective of how hard the detection of particles due to their lifetime is.

[1] In general, the fermions have non integer spin and the bosons have integer spin

Table 1.1 SM particle properties: mass, charges, spin, lifetime and distance traveled in a lifetime (assuming speed of v=0.998c)[5]. In the case of s,c and b quarks, the lifetime corresponds to the $K^{\pm}$, $D^{\pm}$ and $B^{\pm}$ meson lifetime.

Particle	Mass (MeV/c^2)	Charge	spin	Lifetime (s)	Distance (m)
Up quark (u)	2.2	$\frac{2}{3}$	$\frac{1}{2}$	Stable	-
Charm quark (c)	1280	$\frac{2}{3}$	$\frac{1}{2}$	1.1×10^{-12}	5.21×10^{-3}
Top quark (t)	173100	$\frac{2}{3}$	$\frac{1}{2}$	5×10^{-25}	2.37×10^{-15}
Down quark (d)	4.6	$-\frac{1}{3}$	$\frac{1}{2}$	Stable	-
Strange quark (s)	96	$-\frac{1}{3}$	$\frac{1}{2}$	1.2×10^{-8}	58.7
Bottom quark (b)	4180	$-\frac{1}{3}$	$\frac{1}{2}$	1.6×10^{-12}	6.16×10^{-3}
W	80379	±1	1	3×10^{-25}	1.4×10^{-15}
Z	91187.6	0	1	3×10^{-25}	1.4×10^{-15}
Photon (γ)	0	0	1	Stable	-
Gluon (g)	0	0	1	Stable	-
Higgs (H)	125180	0	0	1.5×10^{-22}	7.39×10^{-13}
Electron (e)	0.511	-1	$\frac{1}{2}$	Stable	-
Muon (μ)	105.7	-1	$\frac{1}{2}$	2.2×10^{-6}	10419.85
Tau (τ)	1776.86	-1	$\frac{1}{2}$	2.9×10^{-13}	1.37×10^{-3}
ν_e, ν_μ, ν_τ	$< 2.0 \times 10^{-6}$	0	$\frac{1}{2}$	Stable	-

1.3 Higgs Boson

The Higgs is a boson with spin 0 and chargeless. First theorized in 1964 by a group of theoretical physicist composed by Peter Higgs, François Englert, Robert Brout, Gerald Guralnik, C. Richard Hagen, and Tom Kibble in separate groups. They formulated the Higgs mechanism that explains the generation of mass for the fermions and massive bosons. The Higgs boson was discovered recently in year 2012 in the experiments ATLAS and CMS at CERN. The experiment was conducted using proton-proton collisions with center of mass energy of 7 and 8 TeV, where investigators analyzed the data in the $\gamma\gamma$ and ZZ final states[6, 7]. The mass of this boson has been measured and its production and decay rates are consistent with the SM prediction. The mass of the Higgs boson measured is 125.18 ± 0.16 GeV[5]. The Higgs boson lifetime is 1.56×10^{-22} s. That is why the Higgs boson was very difficult to detect in particle detectors.

1.4 Top quark

The top quark is the most massive particle with a charge of 2/3 and spin of 1/2. First proposed by M. Kobayashi and T. Maskawa in 1973 to explain observed CP violations in Kaon decay[1]. In 1995, in the Tevatron at Fermilab in Illinois, the top quark was discovered via proton antiproton collisions with center of mass energy between 1.8 to 1.96 TeV in the CDF and D0 experiments. The top quark production process was via ggF, which generated a pair of $t\bar{t}$[8]. Since then, the properties of the top quark have been studied at the Tevatron Collider at Fermilab, and by the ATLAS and CMS experiments at the Large Hadron Collider (LHC) at CERN. However, the top quark often receives special attention in new physics models because its mass requires near unity coupling to the Higgs boson[8]. As shown in Table 1.1, the top quark lifetime is so small that they decay before they can hadronise, that is to say, the process to create hadrons from quarks and gluons.

One of the interesting properties of top quark is its mass. The top quark mass is a free parameter in the SM and was extracted using indirect measurements and relying on SM calculations. The measured value of the top quark mass is of 173 Gev[5]. The top quark mass is a very important parameter that puts a constraint in the Higgs boson mass and also takes an important role in electroweak symmetry breaking[8].

The production of top quark can be generated in different ways. In Tevatron and LHC, the production of $t\bar{t}$ comes mainly from ggF (gluon gluon fusion) via strong force. Even it is possible to create a single top quark in the LHC via electroweak interactions (with a W boson)[9]. The top quark, due to its big mass, always decays into a W boson and a b quark. But since the W boson has various decays, the top quark can generate many possible particles, according to W boson decays. Some possible decay of the top quark is the decay to a lepton such as muon, electron or tau and their neutrinos.

1.5 Higgs mechanism

In the SM, mathematically the particles are described in form of fields. The SM for electroweak interactions is described as a gauge theory with a symmetry group SU(2)⊗U(1) that describes the weak and electromagnetic interactions due to the exchange of spin 1 gauge fields($W^{\pm}$,Z) for the weak part and a photon for the electromagnetic part. The Higgs mechanism give bosons and fermions their mass. The lagrangian for the electroweak part of SM

$$\mathscr{L}_{\text{EW}} = \mathscr{L}_{\text{gauge}} + \mathscr{L}_f + \mathscr{L}_{\text{Higgs}} + \mathscr{L}_{\text{Yukawa}} \tag{1.1}$$

The first term of the lagrangian refers to gauge bosons

$$\mathscr{L}_{\text{gauge}} = -\frac{1}{4}\left[F^{\mu\nu}F_{\mu\nu}\right] - \frac{1}{4}\left[\sum_i G^{i\mu\nu}G^i_{\mu\nu}\right] \tag{1.2}$$

where the F and G are[2]

$$F^{\mu\nu} = \partial_\mu B_\nu - \partial_\nu B_\mu \tag{1.3}$$

$$G^{i\mu\nu} = \partial_\mu W^i_\nu - \partial_\nu W^i_\mu - g\varepsilon^{ijk}W^j_\mu W^k_\nu \tag{1.4}$$

W^i (i=1,2,3) are three SU(2) gauge bosons, B is a U(1) gauge boson and g is a couping constant for W gauge boson. In the end, a superposition of these gauge bosons, after introducing the Higgs mechanism, become the $W^{\pm}$, Z and γ vector boson [10, 11].

The second term refers to kinetic energy of fermions

$$\mathscr{L}_f = \sum_{m=1}^{3}\left(\bar{q}^m_L i\not{D}_L q^m_L + \bar{l}^m_L i\not{D}_L l^m_L + \bar{u}^m_R i\not{D}_R u^m_R + \bar{d}^m_R i\not{D}_R d^m_R + \bar{e}^m_R i\not{D}_R e^m_R\right) \tag{1.5}$$

[2] ε^{ijk} represents the Levi-Civita tensor, where $\varepsilon^{ijk} = \begin{cases} +1 & \text{for even permutation} \\ -1 & \text{for odd permutation} \\ 0 & \text{i=j, or j=k, or k=i} \end{cases}$.

where m is the family index, and L(R) refer to the left (right) handed particles.[3] The gauge covariant derivatives are given by

$$D_L = \left(\partial_\mu + ig\sigma^i W_\mu^i + ig' Y B_\mu\right) \tag{1.6}$$

$$D_R = \left(\partial_\mu + ig' Y B_\mu\right) \tag{1.7}$$

where σ^i are the Pauli matrices and g' is the coupling constant for B gauge boson. The left handed fields for the first family are defined by the following doublets

$$q_L = \begin{pmatrix} u_L \\ d_L \end{pmatrix} \qquad l_L = \begin{pmatrix} \nu_{eL} \\ e_L^- \end{pmatrix} \tag{1.8}$$

and the right handed fields

$$u_R, d_R, e_R^- \tag{1.9}$$

The hypercharges Y depend of the particle type. For left handed

$$Y(l_L) = -\frac{1}{2} \quad Y(q_L) = \frac{1}{6} \tag{1.10}$$

for right handed

$$Y(e_R) = -1 \quad Y(u_R) = \frac{2}{3} \quad Y(d_R) = -\frac{1}{3} \tag{1.11}$$

The lagrangian for Higgs field

$$\mathscr{L}_{\text{Higgs}} = (D_\mu \Phi)^\dagger (D^\mu \Phi) - V(\Phi^\dagger \Phi) \tag{1.12}$$

where D_μ is an operator

$$D_\mu = \left(\partial_\mu + i\frac{1}{2}\sigma^i g W_\mu^i + i\frac{1}{2} g' B_\mu\right) \tag{1.13}$$

and the Higgs potential $V(\Phi^\dagger \Phi)$

$$V(\Phi^\dagger \Phi) = \mu^2 \Phi^\dagger \Phi + \frac{1}{2}\lambda (\Phi^\dagger \Phi)^2 \tag{1.14}$$

[3] $\bar{\psi}$ denotes the adjoint spinor $\bar{\psi} = \psi^\dagger \gamma^0$. $\not{D} = \gamma^\mu D_\mu$. γ are the Dirac matrices

$\Phi = \begin{pmatrix} \phi^+ \\ \phi^0 \end{pmatrix}$ is a SU(2) doublet of scalar fields. V is symmetrical under rotations in Φ space and parameters λ and μ^2 are parameters of the potential. The Higgs potential for $\mu^2 < 0$ and $\lambda > 0$ can be visualized in Figure 1.3

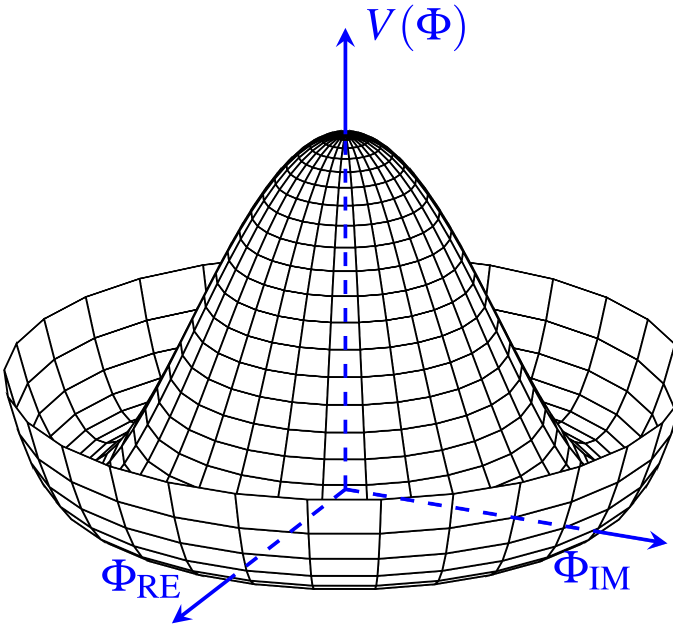

Fig. 1.3 Higgs potential $V(\Phi^\dagger\Phi)$ for $\mu^2 < 0$ and $\lambda > 0$

Electroweak symmetry breaking refers to the choice of ground state

$$\Phi_0 = \frac{1}{\sqrt{2}} \begin{pmatrix} 0 \\ v \end{pmatrix} \tag{1.15}$$

where $v = -\frac{\mu^2}{\sqrt{2}}$ is called the vacuum expectation value.

Taking 1.15 and substituting in $\mathscr{L}_{\text{Higgs}}$, we get

$$(D_\mu\Phi)^\dagger(D^\mu\Phi) = \frac{v^2}{8}\left(g^2((W_\mu^1)^2 + (W_\mu^2)^2) + (gW_\mu^3 - g'B_\mu)^2\right) \tag{1.16}$$

we define the physical vector boson W_μ^-, W_μ^+ and Z_μ

$$W_\mu^\pm = \frac{1}{\sqrt{2}}(W_\mu^1 \mp iW_\mu^2) \tag{1.17}$$

$$Z_\mu = \frac{1}{\sqrt{g^2 + g'^2}}\left(gW_\mu^3 - g'B_\mu\right) \tag{1.18}$$

Now introducing 1.17 and 1.18 in 1.16,

$$(D_\mu\Phi)^\dagger(D^\mu\Phi) = \frac{v^2}{8}\left(2g^2W_\mu^+W^{\mu-} + (g^2+g'^2)Z_\mu Z^\mu\right) \tag{1.19}$$

from the coefficients, we get the W and Z mass

$$m_W = \frac{gv}{2} \qquad m_Z = \frac{v}{2}\sqrt{g^2+g'^2} \tag{1.20}$$

The last part of the lagrangian is the Yukawa lagrangian[4]

$$\mathscr{L}_{\text{yukawa}} = \sum_{m,n}^{3} \Gamma^u_{mn}\bar{q}_{m,L}\tilde{\Phi}u_{n,R} + \Gamma^d_{mn}\bar{q}_{m,L}\Phi d_{n,R} + \Gamma^e_{mn}\bar{l}_{m,L}\Phi e_{n,R} + h.c \tag{1.21}$$

The matrices Γ_{mn} describe the so called Yukawa couplings between Higgs doublet Φ and the fermions. The indices m and n mean sum over the families. By using 1.15 on $\mathscr{L}_{\text{yukawa}}$, it is obtained for u quark

$$\frac{\Gamma^u_{uu}v}{\sqrt{2}}(\bar{u_L}u_R + \bar{u_R}u_L)$$

from which the masses for the fermions are shown to be proportional to the Yukawa couplings

$$m_u = -\frac{\Gamma^u_{uu}v}{\sqrt{2}}$$

[4]Here $\tilde{\Phi} = i\sigma^2\Phi^\dagger = \begin{pmatrix} \phi^{0^\dagger} \\ -\phi^- \end{pmatrix}$ is necessary for the correct transformation in the case of up-type quarks. h.c refers to hermitian conjugate terms.

1.6 Higgs production mechanisms

During a particle collision, there are various ways that the Higgs boson can be created. The most common is the gluon gluon fusion process (ggF) which is the process which involves two gluons mediated by the exchange of a virtual, heavy top. quarks. Another process is vector boson fusion (VBF), where two fermions interact via a vector boson (W or Z) and create a Higgs along with other particles. There is also the vector Higgs process (VH), where the creation of particles using vector boson comes from a interaction between fermions and anti fermions[5]. These processes are shown in the Figure 1.4

In the recent years, people have studied the top anti top Higgs ($t\bar{t}H$) process, in order to detect a Higgs boson, via multilepton signals[9]. In this process, the creation of a Higgs boson comes from a interaction via $t\bar{t}$. In the Figure 1.4, the $t\bar{t}H$ starts with 2 gluons which decay to two $t\bar{t}$ pairs and after that, the interaction $t\bar{t}$ generates a Higgs. The last process, subject of study in this thesis, is the top Higgs (tH) process. This process is a rare expected process with a very small production rate[5].

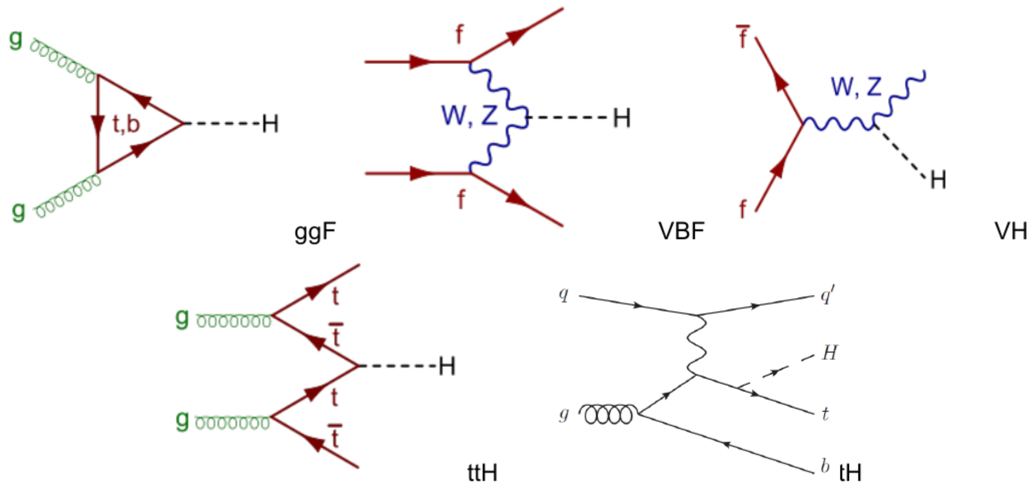

Fig. 1.4 Different Higgs production mechanism, from the most likely to least likely [12][13]

In the tH process, a Higgs boson is radiated from a single top quark as shown in Figure 1.4. The tH process has gained interest recently[9], given that there are few experiments and its production rate (probability) is small, so the detection of Higgs bosons in this channel opens the path to new discoveries.

In particle physics, cross section (σ) describes the likelihood of two particles interacting under certain conditions. Cross sections are expressed in barns, where 1 barn=10^{-34} cm^2. The cross section is important in the evaluation of events for specific processes. In order to get the number of events for a specific process, the reaction rate N is determined by the total cross section σ and the luminosity L[5].

[5]The unit of measurement of instantaneous luminosity is cm^{-2}s^{-1}.

Therefore, the reaction rate is

$$N_R = \sigma \mathrm{L} \tag{1.22}$$

In practice, the luminosity is measured by counting the number of events for a well known process.

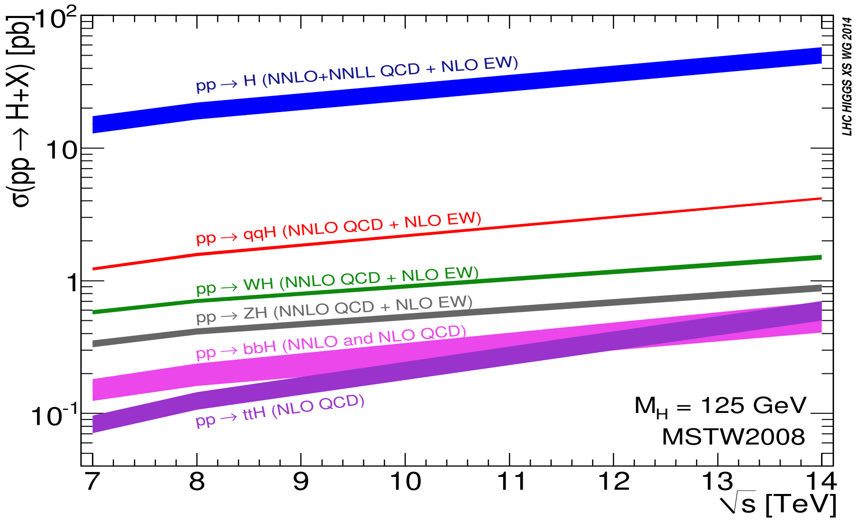

Fig. 1.5 Cross section for different processes generated in a pp collision [14]

Table 1.2 Higgs boson production cross sections in pp collisions for $\sqrt{s} = 13$TeV (in pico barn) and number of events for an integrated luminosity of 35.9 fb^{-1} for Run 2 [5]

Production mechanism	σ (picobarns pb)	Number of events
ggF	48.93	1756587
VBF	3.78	135702
WH	1.35	48465
ZH	0.88	31592
$t\bar{t}$H	0.50	18255
tH	0.074	2655

Table 1.2 shows the Higgs production cross section for pp collisions and the number of events produced using a integrated luminosity of $35.9 fb^{-1}$, that is the luminosity measured for the Run 2 from LHC on 2016[5]. Figure 1.5 shows the cross sections for each Higgs mechanism process that comes from pp collisions in relation to colliding energy. Here we can see that the ggF process has the biggest cross section of all Higgs mechanism and generates the greatest number of events possibles. For the processes tH and $t\bar{t}$H, they have the smallest cross section, so the probability for the processes is low and generates a small number of events.

1.7 Higgs decay rates

In particle physics, two important properties are the lifetime and the decay rates of a particle. The lifetime is related to the total decay rate Γ, that is the probability per unit of time a particle will decay,

$$dN = -\Gamma N dt \tag{1.23}$$

with N the original number of particles before the decay. From here is evident that number of particles left in a decay is

$$N(t) = N_0 e^{-\Gamma t} \tag{1.24}$$

The number of particles decreases over time exponentially and this can be measured. With this, it is possible determine the mean lifetime[1]

$$\tau = \frac{1}{\Gamma} \tag{1.25}$$

In case of the decay rate to a specific process, it is necessary to get the branching fraction of the process. The branching ratio for a decay process is the ratio of the number of particles which decay via a specific decay mode with respect to the total number of particles which decay via all decay modes.

$$BR_i = \frac{\Gamma_i}{\sum_i \Gamma_i} \tag{1.26}$$

Where $\Gamma = \sum_i \Gamma_i$ is the total decay width (sum of all partial widths) of the particle. The lifetime of the Higgs boson is predicted to be 1.56×10^{-22} seconds and corresponds to Γ_H of about 4 MeV, but has not yet been measured due to the detector resolution[15].

Table 1.3 SM Higgs boson branching ratios for M_H =125 GeV [5]

Higgs decay	Branching ratio (BR)
$H \to b\bar{b}$	58.4%
$H \to W^+W^-$	21.4%
$H \to \tau^+\tau^-$	6.27%
$H \to ZZ$	2.62%
$H \to \gamma\gamma$	0.227%
$H \to Z\gamma$	0.153%
$H \to \mu^+\mu^-$	0.0218%

The decay $H \to b\bar{b}$ has a branching ratio a bit more than 50%. The decay $H \to \mu^+\mu^-$ has a very low branching ratio. This decay is very rare but not impossible to detect in the future.

1.8 *tH* production mechanism

The production of *tH*, where a Higgs boson can be radiated either from the top quark or from the exchanged *W* boson in the two dominant leading order diagrams shown in Figure 1.6 provides a unique opportunity to study the relative sign of the Higgs top coupling. In practice, we do not directly measure the Yukawa couplings. Instead, modifier parameters k_t and k_V are introduced in the analysis to represent deviations from the Yukawa coupling values described in Section 1.5. In the SM, the two diagrams interfere negatively and thereby suppress the production cross section. Any deviation from the SM coupling parameters can lead to a large enhancement of the event rate. In this proje[illegible]onsider a modified model with k_t=-1, which leads to a con[illegible] cross section more than ten times

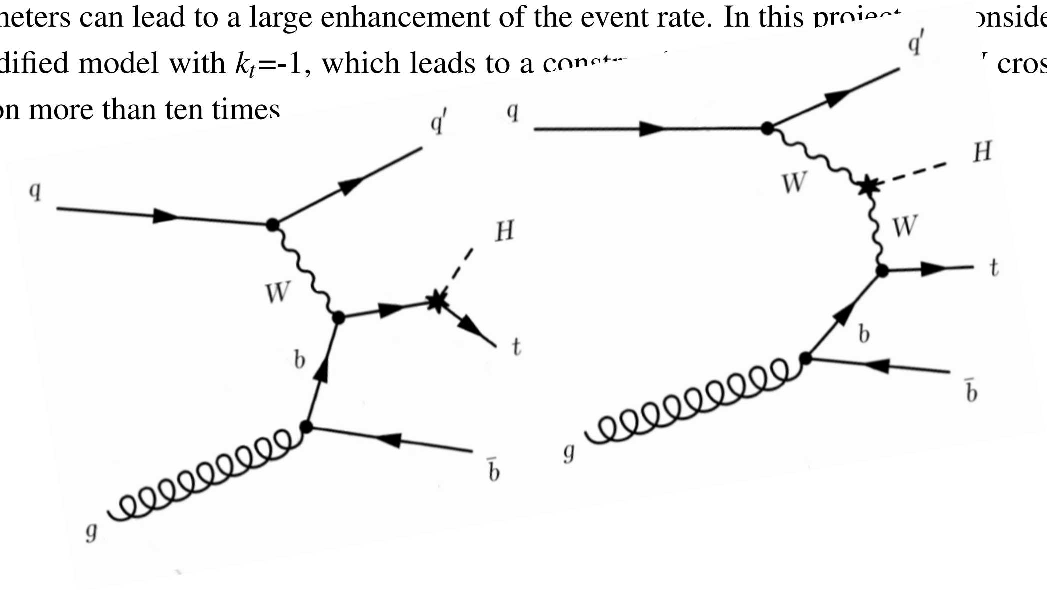

Fig. 1.6 *tH* mechanism. Higgs radiated from a top quark (left). Higgs radiated from a W boson (right) [16]

Chapter 2

The LHC and CMS

2.1 The Large Hadron Collider

The LHC is the largest and most powerful particle accelerator in the world. It came on operation on 10 September 2008 and it is the most recent addition from the European Organization for Nuclear Research (CERN). The LHC is a 27 kilometer ring composed of superconducting magnets with accelerating structures to boost the energy of the particles.

The LHC is designed to accelerate particles to high energies and generate collisions. There are several experiments installed along the LHC ring as shown in Figure 2.1. One of them is ATLAS, located on Point 1 between the two injection lines, which is a general purpose detector. At point 5 is another general purpose detector: the compact muon solenoid (CMS). A particle detector optimized for heavy ion physics, ALICE, is located at Point 2 and LHCb, a detector designed for B physics, is located at Point 7[17, 18].

Inside the accelerator, two high energy particle beams travel at close to the speed of light before they collide. In order to make them collide, beams travel in opposite directions in separate beam pipes, two tubes kept at ultrahigh vacuum. By using superconducting electromagnets that generate a powerful magnetic field, the beams are guided around the accelerator ring. The electromagnets are built from coils of special electric cable that operates in a superconducting state, efficiently conducting electricity without resistance or loss of energy. For that, it is required to have magnets at a temperature of -271.3 C. To reach such temperatures, a system of liquid helium is connected to the accelerator[18].

Protons in the LHC start out as hydrogen atoms stripped of their electrons. The first accelerating stage the protons are subjected to is a linear accelerator, Linac2, which accelerates them up to 50 MeV. The protons are then sent into the Proton Synchotron Booster which accelerates them up to 1.4 GeV before sending them to the Proton Synchotron (PS). The protons leave the PS at 25 GeV before entering the Super Proton Synchotron (SPS),

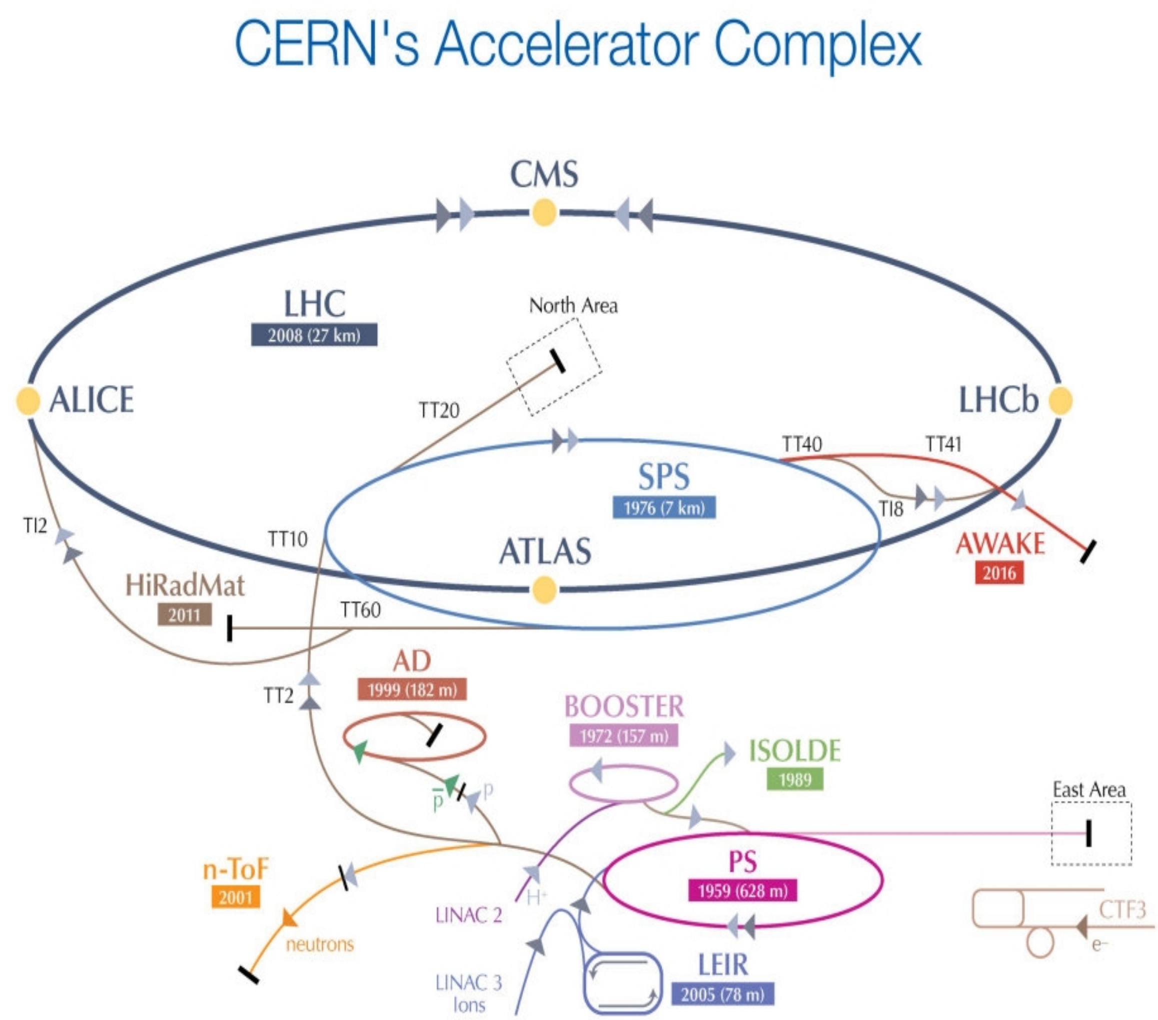

Fig. 2.1 CERN accelerator complex [17]

which accelerates them to the LHC injection energy of 450 GeV. After this stage, the beam is ready to be injected into the LHC through one of two injection lines with 6.5 TeV[19].

Inside the detectors, colliding protons generate an amount of particles such as pions and kaons, which are the most common, created by the jet particles that were produced after the collision. Besides the particles created by the quarks of the proton, gluons are also radiated and create new particles and photons are radiated too. Within a short time, the main detectors of LHC capture and save the data using high performance computing.

The main objective of the LHC is to study the nature of electroweak symmetry breaking for the Higgs mechanism of the SM. Alternatives to the Standard Model that involves different symmetries are also put to test. With the exploration of theses theories, people hope for a discovery that guides them towards a unified theory, so the importance to accelerate particles to higher energy scales and high intensity experiments.

The LHC has a schedule where there is a period of experiments that last for three or four years. Ending the experimental time, the engineers of the LHC start the maintenance.

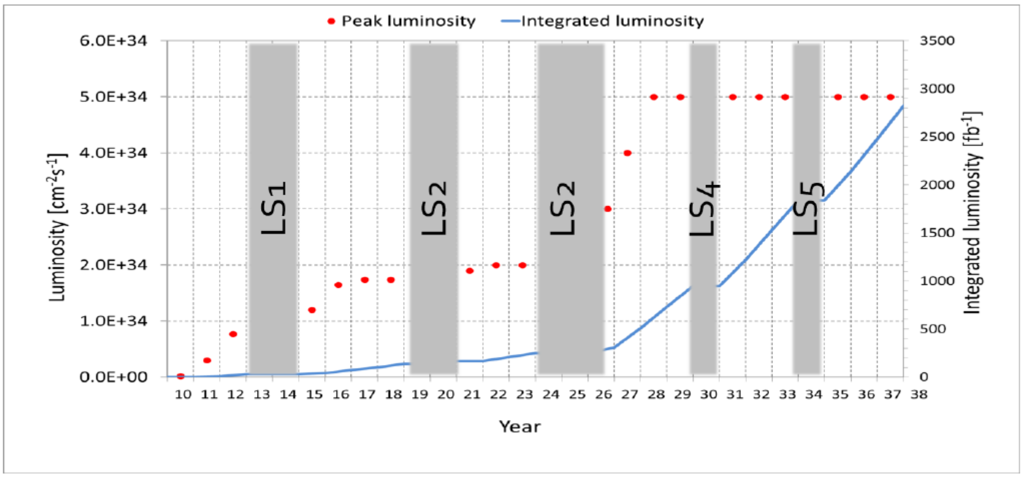

Fig. 2.2 LHC schedule, including future plans for increase the center of mass energy and luminosity. The periods labeled LS are the maintenance periods[19].

Figure 2.2 shows the Large Hadron Collider forecast for the increase of luminosity for the next years. Red dots represent the expected peak luminosity and blue line shows the expected luminosity. In the year 2018, the maximum integrated luminosity is around 150 fb^{-1}[19]. From 2019 to 2021 the second phase of maintenance will take place, where engineers increase the performance of the accelerator, give maintenance to the system and introduce new components to the complex. After that period, the LHC will start a new collision period at even higher energies in order to explore new particle phenomena.

2.2 The Compact Muon Solenoid

The Compact Muon Solenoid (CMS) is a detector with multiple uses in the LHC and part of the main experiments at CERN. It is located underground in the France- Switzerland border, in the city of Cessy, France. This detector was designed in the early 1990s, based on the mass limit of the Higgs boson, and put on operation in 2008. It has a big solenoid that generates a great magnetic field of 4 teslas with the objective of separating particles after a particle collision. The detector is 21 meters long, 15 meters wide, 15 meters high, it has a diameter of 5.9 m with a weight of 12000 ton. The reason for such a strong magnetic field is to obtain a better momentum resolution. More characteristics of the solenoid are shown in Table 2.1.

Table 2.1 Characteristic of the CMS superconducting solenoid[15]

Field strength	4 T
Inner Bore	5.9 m
Length	12.9 m
Number of Turns	2168
Current	19.5 kA
Stored energy	2.7 GJ

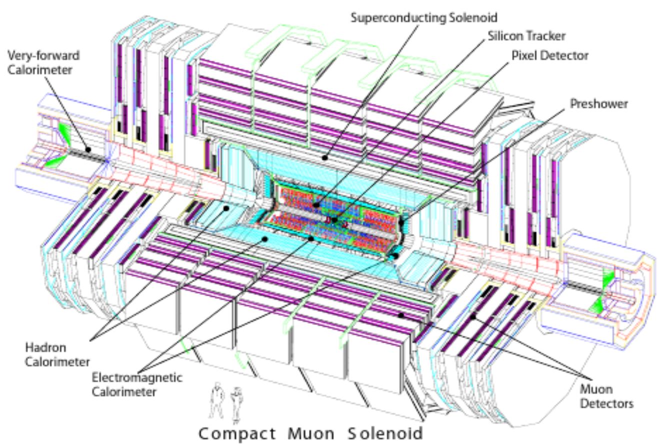

Fig. 2.3 View of Compact muon solenoid (CMS)[15]

The CMS experiment is composed of several detector layers that allow identify and save different types of energy signals and it is saved in a powerful supercomputers that separate and classify the data according to certains variables. The general parts of the CMS are the Silicon Tracker, an Electromagnetic Calorimeter, a Hadron Calorimeter, the solenoid (superconducting magnet) and the Muon Detector. All these parts are illustrated in Figure 2.3.

The objectives of the CMS experiment are numerous. One of them is the identification of muons by measuring the momenta and scattering angle. Muons can be produced in interesting events like Higgs, $W^{\pm}$ and Z boson decays. This experiment along the ATLAS experiment discovered the Higgs boson in 2012.

2.2.1 Silicon Tracker

The Silicon Tracker is the first of the main subdetectors of CMS from inside to outside. The Tracker is composed of two sub components: Pixel and Strip detectors. The outer radius of the tracker is 110 cm, and its total length is 540 cm. The tracker coverage is $|\eta| < 2.4$[1].

In the Pixel barrel section, there are 3 layers of pixel sensors with radii of 4.4, 7.3 and 10.2 cm with a length of 53 cm. Each pixel has an area of 100 $\times$ 150 μm^2. The barrel section has 768 pixel modules. The Pixel endcap has 2 disks on each side placed at 34.6 and 46.5 cm in the z axis. Each disk covers radii from 6 to 15 cm and is divided into 24 blades with 7 modules each. They are assembled in a turbine-like geometry that contains a total of 672 pixel modules.

The Strip Detector is divided in 4 sections: Tracker inner barrel (TIB), tracker outer barrel (TOB), tracker encap (TEC) and tracker inner disk (TID). The region that covers the barrel section is $|z| < 65$ cm for TIB and $|z| < 110$cm for TOB. The first two are composed of silicon sensor layers of 4 and 6 layers respectively. The TEC has 9 disks extending in the region 120 cm > $|z|$ > 280 cm. The TID comprises 3 small disks that fill the gap between the TIB and the TEC.

The Strip Detector has almost 15 400 modules, mounted on carbon-fiber structures and housed inside a temperature controlled outer support tube. The operating temperature must be around -20°C. The total area of the pixel detector is around 1 m^2 and the silicon strips is 200 m^2. The inner tracker comprises 66 million pixels and 9.6 million silicon strips [15]. A full coverage of the Tracker is shown in Figure 2.4

The particle collision generates a lot of different particles that pass first through the inner tracker, interacting with the sensor layers and registering the particle path. By reconstructing the path of the particles, it is possible to generate a track, which allows to measure the momentum of the particle by calculating its curvature. The tracker is used to reconstruct the path of charged particles (e.g. electrons, muons, pions). The most important objects of study are the momentum and the vertex (origin of the track). The efficiency of the tracker is estimated by using samples of muons and pions with p_t that is the transverse

[1] η, called pseudorapidity, is a coordinate where $\eta = -\ln\tan\frac{\theta}{2}$ with θ is the angle between the particle momentum p and the direction of the beam axis

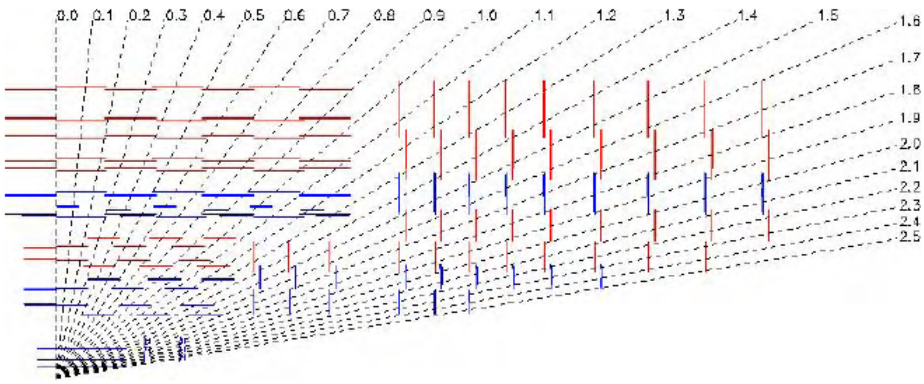

Fig. 2.4 The Tracker layout distributed in terms of η[15].

momentum (component of momentum transverse to beam line) of 1,10 and 100 GeV. For muons the efficiency of the tracker is shown in Figure 2.5

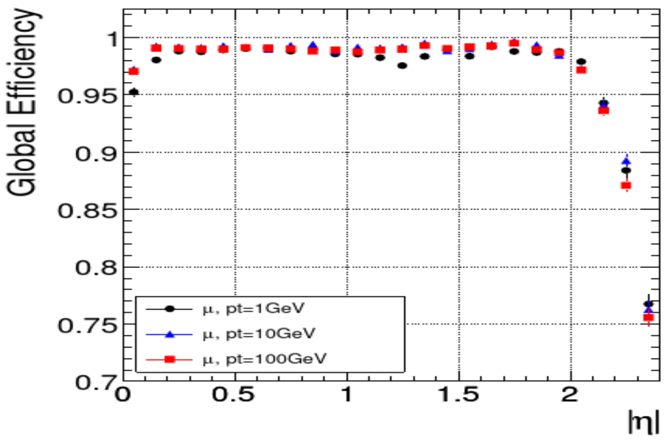

Fig. 2.5 Total reconstruction efficiency for muons[15]

According to Figure 2.5, the efficiency of the tracker is around 98 % for $|\eta| < 2$. The resolution of the tracker for muons with p_t=100 GeV is around 1-2 %. Of course, this is a first stage of the measurement of particle momentum because the other detectors are used to increase and improve the measurement and reconstruction of the particle path.

2.2.2 Electromagnetic calorimeter

The electromagnetic calorimeter or ECAL is a calorimeter composed of 61200 lead tungstate ($PbWO_4$) crystals that act as scintillating crystals (emit light when particles interact with the crystal). These calorimeters are mounted in the central barrel and closed by 7324 crystals in both endcaps. The barrel section of the ECAL covers the range $|\eta| < 1.479$. The crystals in the barrel have a pyramidal shape and their cross section is

22×22 mm^2 at the front face and 26×26 mm^2 at rear face. The crystal length is 230 mm. The EB (barrel section of ECAL) has an inner radius of 129 cm[15]

The endcaps cover the range $1.479 < |\eta| < 3.0$. The distance between the interaction point and the endcap is 3.144 m. The endcap has identically shaped crystals grouped in mechanical units of 5x5 crystals. The crystal cross section for the rear face is 30×30 mm^2, and for the face is 28.62×28.62 mm^2 with length of 220 mm. The ECAL is illustrated in Figure 2.6.

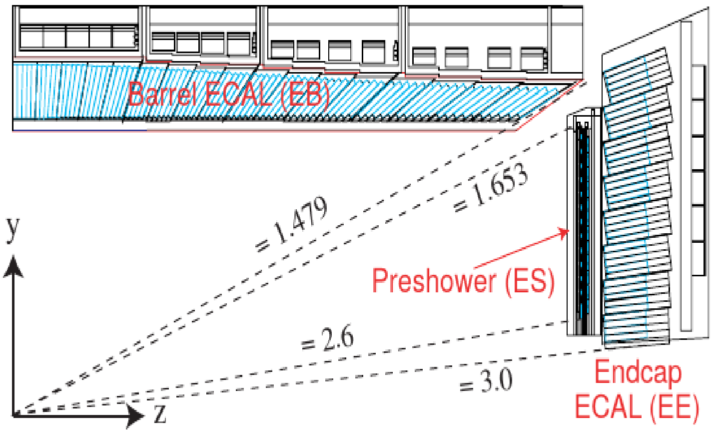

Fig. 2.6 View of the ECAL[15]

In the barrel, there are photo detectors called avalanche photo diodes (APD), made of silicon with an active area of 5×5 mm^2 with 2 glued to the back of each crystal. At the endcap, the photo detectors are vacuum photo diodes (VPT), made of an anode of copper mesh (10 μm), allowing operation in the magnetic field. VPT have a size of 25 mm in diameter, glued to the back of each crystal.

There is also a preshower detector, which principal function is to identify neutral pions in the endcaps within the region $1.653 < |\eta| < 2.6$. It also helps the identification of electrons against minimum ionizing particles, and improves the position determination of electrons and photons.

As its name says, the ECAL is mainly used for the electron detection, but also detects, photons, and neutral pions. The charged particles reach the crystals, create a shower of secondary electrons and photons. The light from the secondary particles is detected by photo diodes. The resolution of the ECAL is estimated by using a test beam and registering the energy signals. The resolution for electrons with energies of 120 GeV is 0.5%.

2.2.3 Hadron calorimeter

The hadron calorimeter (HCAL) together with the ECAL, form a complete calorimeter that allows to measure jets and missing transverse energy. HCAL is located in the barrel and the endcaps, surrounding the ECAL and affected by the magnetic field generated by the solenoid. The Barrel section (HB) and endcap section (HE) cover the pseudorapidity $0 < |\eta| < 1.3$ and $1.3 < |\eta| < 3.0$ respectively. Figure 2.7 shows the structure of the HCAL.

The HB is an assembly of two half barrels, composed of 18 wedges. Each wedge has 17 active layers composed of scintillator tiles with 16 layers of absorber metal (brass and stainless steel). Each tile has a size of $\Delta\eta \times \Delta\phi = 0.087 \times 0.087$. Light of scintillator is collected by a single wave length shifting fiber (WLS) for each scintillator tile. The wedge has a inner radius of 1777 mm and an outer radius of 2876.5 mm.

HE is composed by brass absorber plates, with the thickness of 78 mm, and a total of 19 scintillator layers with a thickness of 3.7 mm. HE is sectioned in 5 in ϕ to match the barrel wedges.

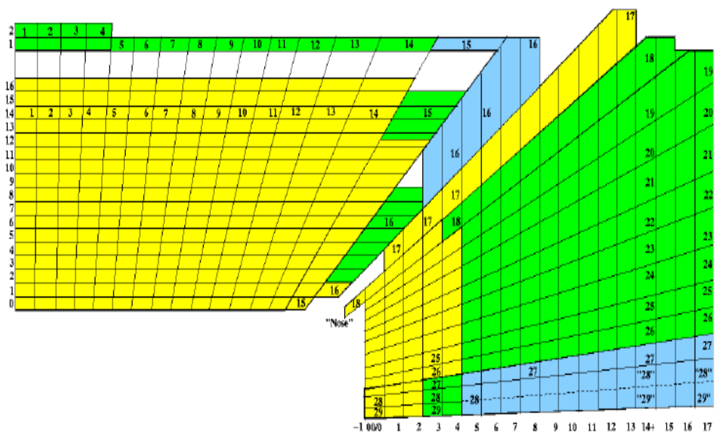

Fig. 2.7 View of the CMS HCAL showing the different layers and tower regions. In the endcap, the towers are defined with two longitudinal segments as shown by the colors[15]

The outer barrel hadron calorimeter (HO) consists of layers of scintillator with thickness of 10 mm, located outside of the magnet coil that cover the region $-1.26 < |\eta| < 1.26$. There is also a forward calorimeter (HF) located at 11.2 m from the interaction point, that cover the region of $2.9 < |\eta| < 5$. They are made of steel absorber and embedded radiation hard quartz fibers, which collect Cherenkov light[15].

The tiles are arranged in a tower pattern in the $\eta - \phi$ space, projective to the interaction point. In total there are 4176 towers. The towers are used as input to several jet reconstruction algorithms.

The HCAL measures the energy of hadrons, such as pions and kaons. The energy resolution of the HCAL was estimated using a test beam of pions. For 100 GeV pions, the resolution obtained is 12%.

2.2.4 Muon Detector

The Muon Detector has three main subdetectors: the drift tube chambers (DT), the cathode strips chambers (CSC) and the resistive plate chamber (RPC). The DT's, CSC's and RPC's are shown in Figure 2.8.

The DT chambers cover the barrel section $|\eta| < 1.2$, composed of rectangular gas filled active cells. Those cells have a transverse size of 42×13 mm^2 with a 50 μm diameter anode wire at the center that operates at voltages of over 3600 V. The gas used in this cells is a mix of Ar and CO_2 with a proportion of 85 % and 15 %, respectively. There are 250 chambers in 4 layers inside the magnet return yoke, with radii of approximately 4.0, 4.9, 5.9 and 7.0 m from the beam axis and 12 sections covering 30° in ϕ each.

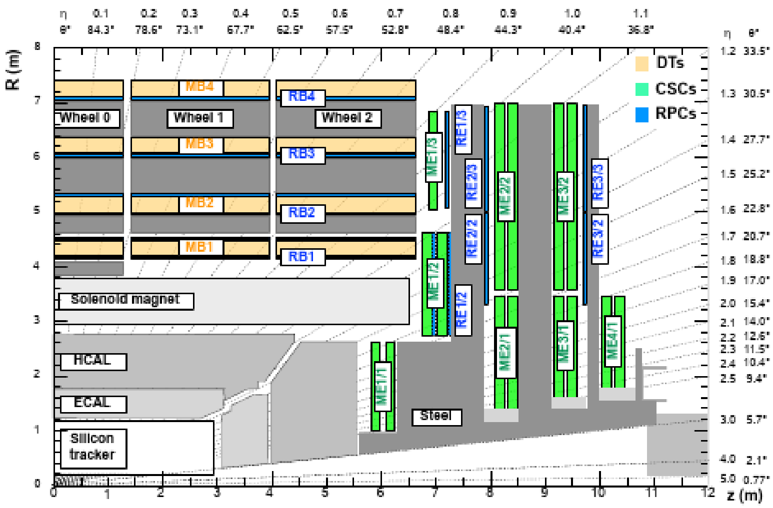

Fig. 2.8 Cross section of a quadrant of the CMS with axis parallel to the beam (z axis) horizontally and the radius of the detector in terms of the η, illustrating the muon detector and its components [15].

The CSC's are located in the endcap regions $0.9 < |\eta| < 2.4$. The CSC's are installed on the face of steel disks perpendicular to the beam. Each CSC has a trapezoidal shape and consists of 6 gas gaps between 7 metal plates, where each gap contains copper cathode strips and anode wires running almost perpendicularly to the strips, with a diameter of 50 μm separated by 3.16 mm. The chambers use a gas mixture of 50% CO_2, 40 % Ar and 10% CF_4. The muon endcap system comprises 468 CSCs in the 2 endcaps [15, 20].

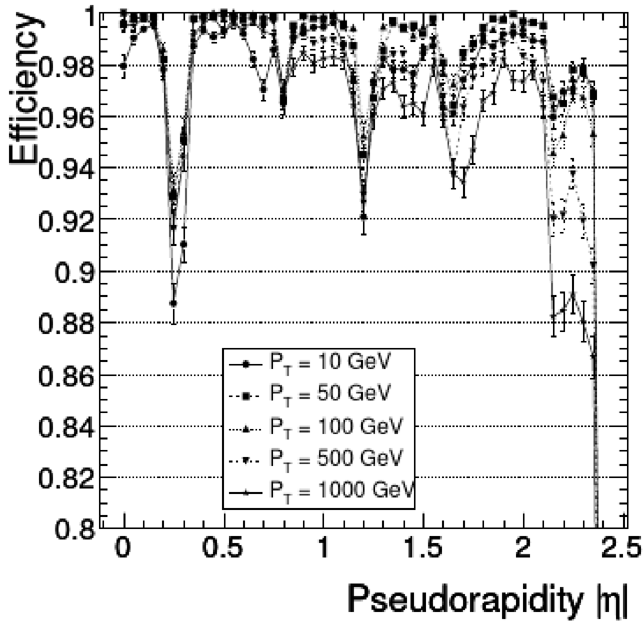

Fig. 2.9 Muon reconstruction efficiency in terms of η and p_t[15]

The RPC are located in the barrel and endcap regions that covers the range of $|\eta| < 1.6$. The main purpose is to trigger events with muons. RPC's are structured with a double gas filled gap and readout strips between the gaps The gas mix used in the RPC consist of 95.2% Freon ($C_2H_2F_4$), 4.5% isobutane (C_4H_{10}), and 0.3% sulphur hexafluoride (SF_6)[20].

The main purpose of the Muon System Detector is to identify muon tracks. The efficiency of the muon system is estimated by using single muon samples simulated with p_t=10, 50, 100, 500 and 1000 GeV. The results are shown in Figure 2.9. The graph shows an efficiency of approximately 98% in the the fully instrumented regions. In the intersection regions, there are drops in efficiency due to the separation of the chambers.

Chapter 3

Event reconstruction and selection

During the proton collision, many types of processes happen whose information is saved in the CMS data storage system. But the events are only saved if they fulfill certain conditions compatible with the signal. For the tH process, the search is based on the presence of a pair of muons with the same sign. The rest of the processes that also generate a pair of muons with the same sign will be considered backgrounds.

The analysis described in this chapter is a summary of the publication from the CMS collaboration using 35.9 fb^{-1} of Run II data [9]. Monte Carlo simulations and event yields shown below, and used in the statistical analysis described in the next chapter, are obtained from this publication.

3.1 Signal Event Topology

In this search, top quark decays to Wb and from the W boson decays to a muon and a neutrino. The Higgs decays to a pair of opposite sign W bosons, where one of the bosons can decay to a μ and its neutrino. b quark creates a b-jet. This is the main process that generates events with two same sign muons. The tH process topology is shown in Figure 3.1. Finally there is a forward quark jet (highest η value) generated from the initial collision. Additional jets or leptons can be generated from the other W boson.

Due to the small cross section of the tH process, the amount of tH events is low compared to other Higgs production processes. Table 3.1 shows several processes that generate same sign muon events for tH. These numbers do not consider the detection efficiency.

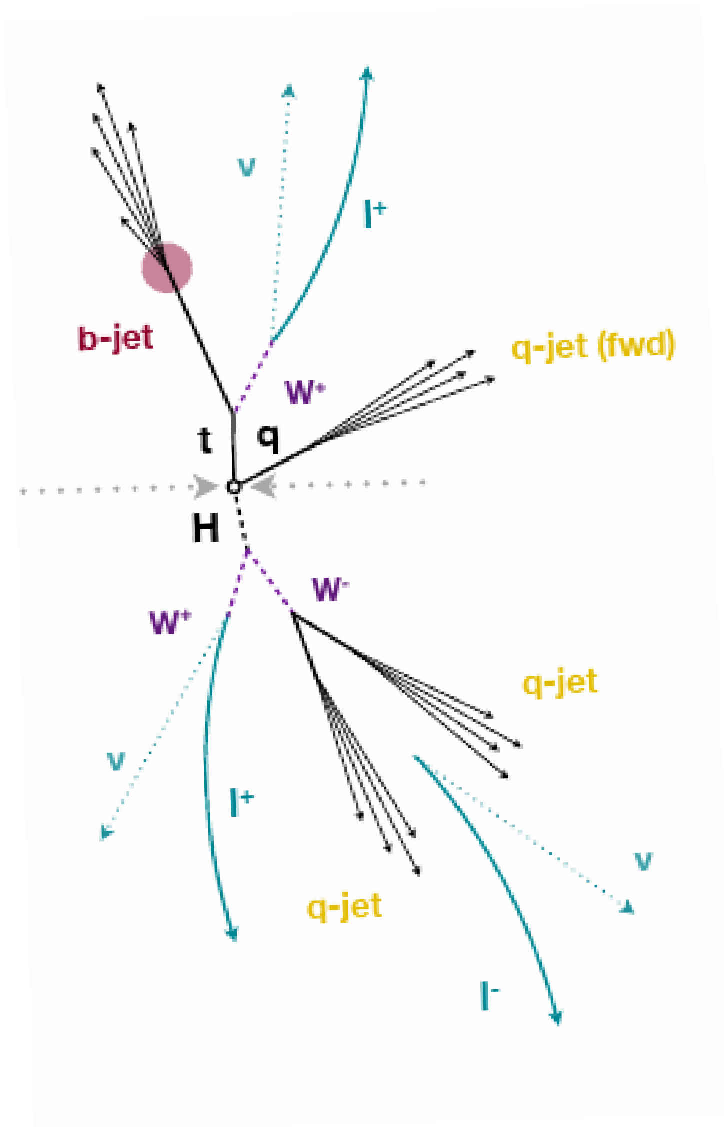

Fig. 3.1 Topology of tH process which generates two same sign muons, a forward jet and a b-jet.

3.2 Backgrounds

Several processes contribute to the background in this search:

- $t\bar{t}W^{\pm}$ and $t\bar{t}Z$ $(t\bar{t}V)$: One muon comes from a top and the other comes from the vector boson.
- $W^{+}Z$: Diboson production with leptonic decays. One muon comes from W boson and the other from Z boson.
- $W^{\pm}W^{\pm}$:A pair of same sign W bosons generate a muon each one.

Table 3.1 Expected number of events for different tH decay chains assuming integrated luminosity of 35.9 fb^{-1}. l represents $\mu^{\pm}, e^{\pm}, \tau^{\pm}$.

Decay chain	BR	Events
$tH \to W^+bW^+W^- \to \mu^+ \nu_\mu b\ \mu^+\nu_\mu\ q\bar{q}'$	2.096×10^{-3}	5.58
$tH \to W^+b\ \tau^+\tau^- \to \mu^+\nu_\mu b\ \mu^+\nu_\mu\bar{\nu}_\tau l^-\bar{\nu}_l\nu_\tau$	3.637×10^{-4}	0.96
$tH \to W^+bW^+\ W^- \to \mu^+\nu_\mu b\ \mu^+\nu_\mu\ l^-\bar{\nu}_l$	3.37×10^{-4}	0.89
$tH \to W^+b\ W^+W^- \to \tau^+\bar{\nu}_\tau b\ \mu^+\nu_\mu\ q\bar{q} \to \mu^+\nu_\mu\ \bar{\nu}_\tau\ \bar{\nu}_\tau b\mu^+\nu_\mu\ q\bar{q}$	1.890×10^{-4}	0.50
$tH \to W^+b\tau^+\tau^- \to \mu^+\ \nu_\mu b\ \nu_\tau\ \mu^+\ \nu_\mu\bar{\nu}_\tau\ q\bar{q}$	1.681×10^{-4}	0.44
$tH \to W^+b\ W^+W^- \to \tau^+\bar{\nu}_\tau b\mu^+\nu_\mu l^-\bar{\nu}_l \to \mu^+\nu_\mu\ \bar{\nu}_\tau\bar{\nu}_\tau b\mu^+\nu_\mu l^-\bar{\nu}_l$	3.045×10^{-5}	0.08
$tH \to W^+bZZ \to q\bar{q}bZZ \to q\bar{q}b\mu^+\mu^-\mu^+\mu^-$	1.966×10^{-5}	0.05
$tH \to W^+b\ \tau^+\tau^- \to \tau^+\bar{\nu}_\tau b\ \mu^+\nu_\mu\bar{\nu}_\tau\ q\bar{q}'\nu_\tau \to \mu^+\nu_\mu\bar{\nu}_\tau\bar{\nu}_\tau b\mu^+\nu_\mu\bar{\nu}_\tau\ q\bar{q}'\nu_\tau$	1.549×10^{-5}	0.04

- $\boldsymbol{tZq}$: Processes with single top quarks associated with a Z boson, where $Z \to \mu^+\mu^-$, also contribute to the background.
- $\boldsymbol{t\bar{t}t\bar{t}}$:In these type of events, one t decays to Wb and W decays to a muon. The second muon comes from the other top decay.
- $\boldsymbol{W^+W^-Z}$, $\boldsymbol{ZZZ}$ and $\boldsymbol{W^+ZZ}$ ($\boldsymbol{VVV}$): The leptonic decays of the W or Z bosons generate at least two same sign muons.
- $\boldsymbol{tZW^+}$:One muon comes from the Z while the other same sign muon can come from t or W.
- $\boldsymbol{ZZ}$: Each muon comes from Z boson decays.
- $\boldsymbol{t\bar{t}H}$: This Higgs production mechanism is considered a background in this analysis. The muons in this case comes from one top and Higgs decays.
- $\boldsymbol{Fakes}$:This background refers to events where two muons come from b meson decays in jets.

Table 3.2 shows the decay chains for the backgrounds. Due to small expected event yields, the processes $W^\pm\ W^\pm$,tZq,$t\bar{t}t\bar{t}$, VVV, tZW^+ and ZZ are grouped as one called Rares in the results below.

3.3 Event Selection

In order to detect signal events and reject background, the following selections are applied, according to the CMS publication[9]

- The events must contain two muons with the same sign.

Table 3.2 Main backgrounds and their same sign $\mu\mu$ decay process

Background	Decay process
$t\bar{t}W$	$t\bar{t}W \to W^+bW^-\bar{b}\ \mu^+\nu_\mu \to \mu^+\nu_\mu b\ \mu^-\bar{\nu_\mu}\bar{b}\ \mu^+\nu_\mu$
$t\bar{t}Z$	$t\bar{t}Z \to W^+b\ W^-\bar{b}\mu^+\mu^- \to \mu^+\nu_\mu b\ \mu^-\bar{\nu_\mu}\bar{b}\mu^+\mu^-$
W^+Z	$W^+Z \to \mu^+\nu_\mu\mu^+\mu^-$
$W^\pm W^\pm$	$W^+W^+ \to \mu^+\nu_\mu\mu^+\nu_\mu$
tZq	$tZq \to W^+\ b\mu^+\mu^-q \to \mu^+\nu_\mu b\ \mu^+\mu^-q$
$t\bar{t}t\bar{t}$	$t\bar{t}t\bar{t} \to W^+b\ W^-\bar{b}\ W^+b\ W^-\bar{b} \to \mu^+\nu_\mu b\ \mu^-\bar{\nu_\mu}\bar{b}\ \mu^+\nu_\mu b\ \mu^-\bar{\nu_\mu}\bar{b}$
W^+W^-Z	$W^+W^-\ Z \to \mu^+\nu_\mu\ \mu^-\bar{\nu_\mu}\mu^+\mu^-$
ZZZ	$ZZZ \to \mu^+\mu^-\mu^+\mu^-l^+l^-$
W^+ZZ	$W^+ZZ \to \mu^+\nu_\mu\mu^+\mu^-l^+l^-$
tZW^+	$tZW^+ \to W^+b\mu^+\mu^-\mu^+\nu_\mu \to \mu^+\nu_\mu b\mu^+\mu^-\mu^+\nu_\mu$
ZZ	$ZZ \to \mu^+\mu^-\mu^+\mu^-$
$t\bar{t}H$	$t\bar{t}H \to W^+bW^-\bar{b}W^+W^- \to \mu^+\nu_\mu b\mu^-\bar{\nu_\mu}\bar{b}\ \mu^+\nu_\mu\ \mu^-\bar{\nu_\mu}$

- Transverse momentum $p_t > 25$ GeV for the highest p_t muon and $p_t > 15$ GeV for the lowest p_t muon.
- A forward jet with $p_t > 40$ GeV and $|\eta| > 2.4$
- One or more b-tagged jets with $|\eta| < 2.4$

The number of expected events after the event selection predicted by the Monte Carlo simulations used in the CMS publication are shown in Table 3.3 which corresponds to a integrated luminosity of 35.9 fb^{-1}[9]. The backgrounds with the most events are $t\bar{t}W^\pm$, $t\bar{t}Z$ and Fakes. For the SM signal tH, the number of expected events is 2.14, while for the inverted coupling scenario ($k_t = -1$) the cross section is enhanced by a factor of approximately 10. These event yields will be used to estimate the signal sensitivity. The yields include statistical uncertainties due to the Monte Carlo (MC) samples and systematic uncertainties as described in Table 3.3.

Table 3.3 Event yields for signal and backgrounds after the event selection for a integrated luminosity of 35.9 fb^{-1}. The uncertainties of yields include statistical and systematic[9]

Process	Number of events
$t\bar{t}W$	68 ± 10
$t\bar{t}Z$	25.9 ± 3.9
WZ	15.1 ± 7.7
Rares	20.9 ± 4.9
Fakes	80.9 ± 9.4
$t\bar{t}H$	24.2 ± 2.1
tH (SM)	2.14 ± 0.13
tH ($k_t = -1$)	26.2 ± 2.2

3.4 Systematic uncertanties

The uncertainties of the yields shown in Table 3.3 include systematic uncertainties due to the following sources, described in the CMS publication[9] and summarized here:

- The uncertainties on $t\bar{t}W$ and $t\bar{t}Z$ event yields are mainly due to the uncertainties of their production cross sections.
- The uncertainty on WZ background is estimated using real data events in a three lepton control region.
- In the Rare background, a 50% of uncertainty is assigned.
- The uncertainty on the Fakes background is estimated using real data in a control region, defined by the muon identification criteria.
- For the Higgs processes tH and ttH, the uncertainty are due to the theoretical parameters (e.g. the strong coupling constant α_s and Parton Distribution Functions (PDF)) used in that simulation.

3.5 Multivariable discriminant

Due to small signal to background ratio caused by the small cross section of tH, a multivariable discriminant, which separates signal from backgrounds, is necessary to optimize the signal sensitivity. The multivariable discriminant is a Boosted Decision Tree (BDT) that takes a set of input features and splits input data recursively based on those features[21]. The features can be a mix of categorical and continuous data. The BDT training is performed using several event variables and was trained to discriminate against $t\bar{t}V$ background, because this background is one of the largest backgrounds. The variables used for the BDT [9] were the following:

- Number of jets with $p_t > 25$ GeV, $|\eta| < 2.4$
- Maximum $|\eta|$ of forward jet
- Sum of lepton charges
- Number of jets with $|\eta| > 1.0$
- $\Delta\eta$ between forward jet and b-jet with highest p_t
- $\Delta\eta$ between forward jet and b-jet with lower p_t
- $\Delta\eta$ between forward jet and closest muon
- $\Delta\phi$ of highest p_t same-sign muon pair
- min ΔR (muon pairs)[1]
- p_t of muon with lower momentum

Figure 3.2 shows the BDT distribution for signal and backgrounds.

[1] $\Delta R = \sqrt{\Delta\eta^2 + \Delta\phi^2}$, where ΔR is the distance in the $\eta\phi$ plane

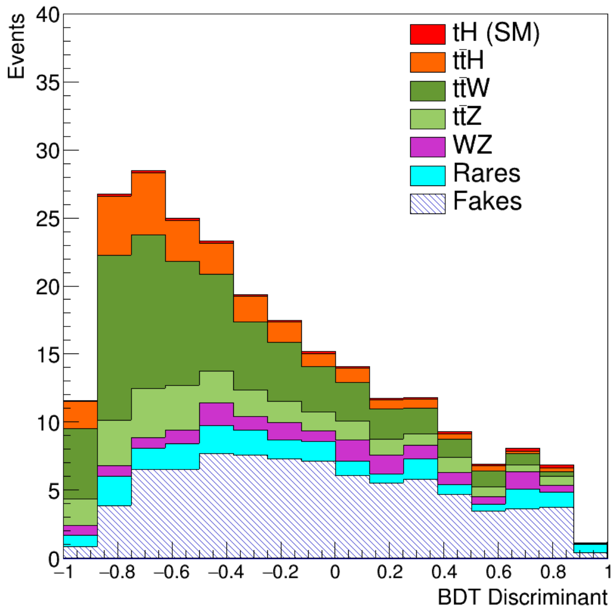

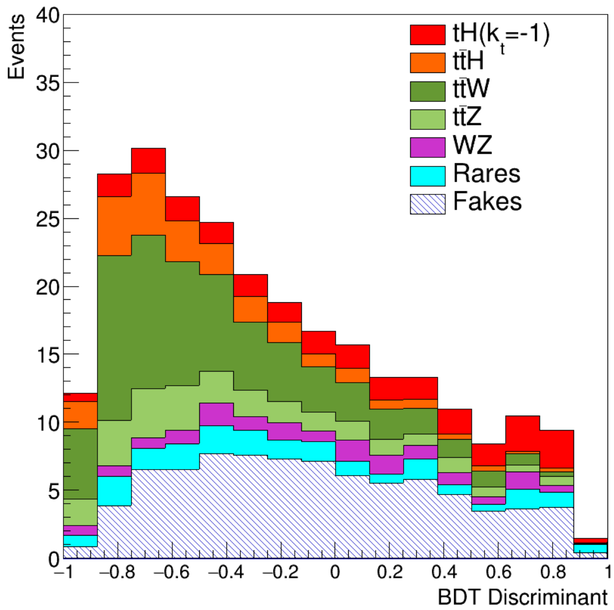

Fig. 3.2 Distribution of BDT discriminant for signal and background in the case of SM (Up) and inverted coupling scenario (Down) [9]

Chapter 4

Statistical Analysis

To estimate the sensitivity of the tH signal, we define an Asimov dataset, made by replacing the ensemble of simulated backgrounds and signal by a single one. The statistical uncertainty of the Asimov data is calculated as $\sqrt{n}$, with n the number of events[22]. The uncertainty of the signal strength is estimated by applying a fit to the Asimov dataset, where the model is constructed from the sum of the individual backgrounds and signal. The fit is implemented using a Poisson likelihood and Gaussian constraints for the systematical uncertainties in the model.

4.1 Likelihood and fit procedure

The likelihood function is the product of Poisson probabilities for all bins of the BDT distribution. The likelihood function has the form

$$L(\mu,\alpha) = \prod_{j=1}^{N} \frac{(\mu s_j + b_j)^{n_j}}{n_j!} e^{-(\mu s_j + b_j)} \prod_{k=1}^{M} e^{\frac{-\alpha_k^2}{2}} \tag{4.1}$$

where N is the total number of bins, n_j is the number of events in a bin j, s_j is the number of signal events, μ is a parameter that modifies the signal strength and b_j is the number of background events. b_j is the sum of different background processes k

$$b_j = \sum_{k}^{M} b_j^k (1 + \alpha_k \sigma_k) \tag{4.2}$$

α_k is the parameter that modifies the expected background prediction and σ_k is the systematic uncertainty of the associated background. σ_k for the backgrounds are shown in the Table 3.3.

The fit is applied by minimizing the negative logarithm of the likelihood function (NLL) with respect to the parameter μ and α_k. The minimization is performed by using programming language ROOT. ROOT is a scientific software toolkit, based on the C++ language, which main objective is the handling of data processing, statistical analysis, including visualization and storage. The package ROOFIT is used here, because of its implementations of modeling probability distributions and statistical tools[23]. Figure 4.1 and Table 4.1, shows the results of the fit to the Asimov data.

As mentioned before, for the k_t=-1 the number of events for signal is more than ten times compared to SM. This improves the sensitivity of the signal. Due to the small number of signal events the uncertainty for the SM is large compared to the k_t=-1 scenario, where the uncertainty is around 50%. In this analysis only the signal is affected by the change k_t=1 (SM) $\rightarrow k_t = -1$, therefore the backgrounds remain the same.

Table 4.2, shows the μ and α parameters. For the pre-fit, values of α are set to zero and μ is set to 1. After the fit, α parameters set to zero indicates that in the fit, the values of the backgrounds did not change for the SM and the μ parameter set to 1 indicates that the signal strength also did not change.

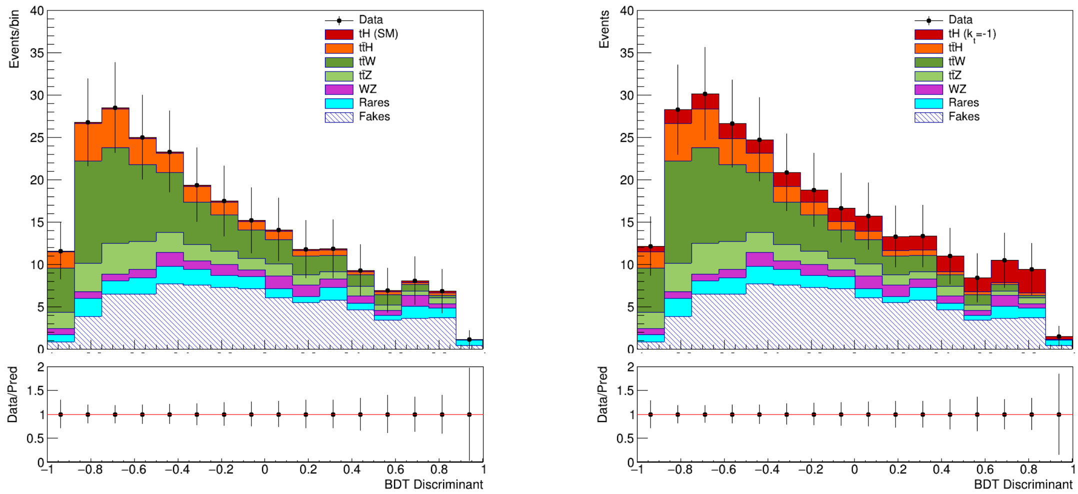

Fig. 4.1 Post-fit signal and background yields for tH process for SM (Left) and $k_t = -1$ (Right).

Table 4.1 Post-fit yields for the fit to the Asimov data corresponding to 35.9 fb^{-1}. The uncertainty given is the combined statistical plus systematic.

Process	SM	k_t=-1
$t\bar{t}W$	68±8.9	68 ±8.9
$t\bar{t}Z$	25.9±3.8	25.9±3.8
WZ	15.1±7.4	15.1±7.4
Rares	20.8±4.8	20.8±4.8
Fakes	80.9±9.0	80.9±8.9
$t\bar{t}H$	24.2±2.0	24.2±2.0
tH	2.1±16.5	26.2±13.1

Table 4.2 α and μ values for the fit to Asimov data corresponding to 35.9 fb $^{-1}$

Parameter	SM	k_t=-1
μ	1.00 ± 7.74	1.0 ± 0.5
$\alpha_{t\bar{t}W}$	0.00 ± 0.89	0.00 ± 089
$\alpha_{t\bar{t}Z}$	0.00 ± 0.98	0.00 ± 0.98
α_{WZ}	0.00 ± 0.97	0.00 ± 0.97
α_{Rares}	0.00 ± 0.95	0.00 ± 0.98
α_{Fakes}	0.00 ± 0.96	0.00 ± 0.95
$\alpha_{t\bar{t}H}$	0.00 ± 0.98	0.00 ± 0.98

4.2 Limit calculation

Due to the large background, the signal strength for the Asimov data with 35.9 fb^{-1} is consistent with zero. Therefore, we estimate an upper limit on the signal strength at 95% confidence level.

We can define the likelihood ratio

$$\lambda(\mu,\alpha) = \frac{L(\mu,\alpha)}{L(\hat{\mu},\hat{\alpha})} \tag{4.3}$$

Where $\hat{\alpha}$ and $\hat{\mu}$ are the parameters obtained in the previous section which correspond to the minimal of the NLL. To determine an upper limit on the strength parameter μ, we use the following statistical test

$$q(\mu,\alpha) = -2\ln\lambda \tag{4.4}$$

High values of q represent greater incompatibility between the data and the fit model. q is a random variable with a χ^2 distribution [22].

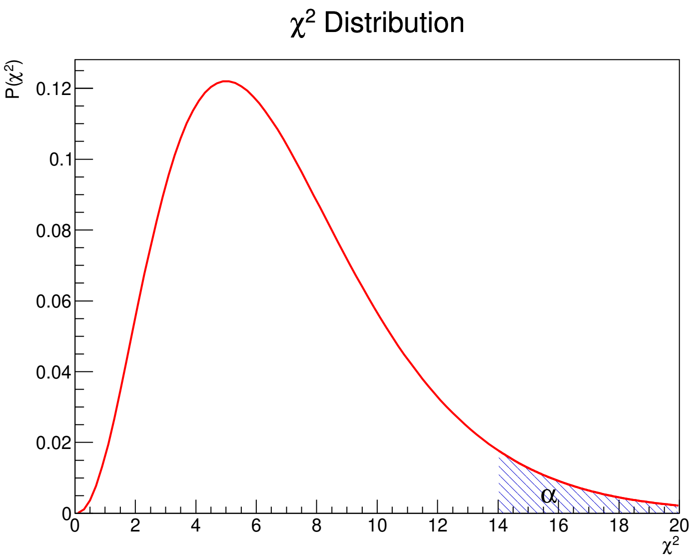

Fig. 4.2 Illustration of the χ^2 distribution with 7 degrees of freedom used for the limit estimation

In order to find the upper limit value of μ, we search for the largest value of μ such that q remains below the shaded region shown in Figure 4.2, where α=0.05 in this case. It is useful to scan q as function of μ, which is normally a parabolic function as shown in Figure 4.3. In the SM case, the scan has a wider shape in comparison to the k_t=-1. This is due to larger statistical uncertainty on the μ parameter. Using the above technique, we find an expected upper limit μ <17.0 for SM model and $\mu < 2.3$ for k_t=-1 model.

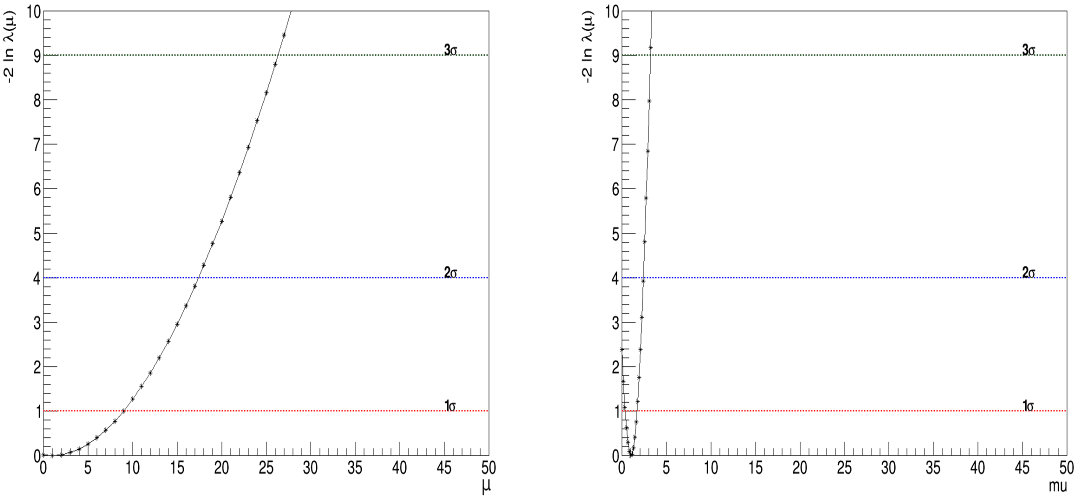

Fig. 4.3 Likelihood scan for SM (Left) and k_t=-1 (Right).

4.3 Extrapolation to higher luminosity

In the past section, it was shown that the signal strength with an integrated luminosity of 35.9 fb^{-1} is not significant. The LHC has already collected data for integrated luminosity of 150 fb^{-1} for run 2 which finished in 2018. Run 3 starts in 2021 and is expected an integrated luminosity of 300fb^{-1} and for the high luminosity phase of LHC, expected to collect 3000 fb^{-1}. Therefore, it is interesting to study the sensitivity of the signal strength at higher luminosity. An extrapolation (scale) is applied to the Asimov data and the statistical uncertainty is adjusted accordingly. For this analysis we assume the systematic uncertainties assigned to the background are the same.

In Figure 4.4, an estimated prediction of the signal and background events for higher luminosity is shown. As the luminosity increases, the number of events for both signal and backgrounds also increases, as previously explained in Chapter 1. But even with the increase of number of events, the statistical uncertainty of the data is too large with respect to the expected signal. In the likelihood scan for higher luminosity, as the luminosity increases, the relative uncertainty on the signal strength μ decreases. This is caused by the increased events available for the fit.

The same method is used for the model k_t=-1 in Figure 4.5. In this case, the number of events for the signal is more appreciable in comparison with the SM model. However, the likelihood scan parabolas are very closed and that indicates a decrease in the uncertainty of μ more notable than SM case. Of course, as the previous section, we estimate the upper limit for these cases and they are shown in the Table 4.3

Table 4.3 Results of μ and upper limits for Asimov extrapolations for SM and k_t=-1 models at 95% confidence level.

Luminosity (fb^{-1})	SM (k_t=1)		k_t=-1 scenario	
	μ	μ upper limit	μ	μ upper limit or interval
35.9	1.0 ± 7.7	17	1.0 ± 0.5	2.3
150	1.0 ± 6.7	11	1.0 ± 0.4	1.8
300	1.0 ± 4.3	8.7	1.0 ± 0.3	1.5
3000	1.0 ± 1.7	4.3	1.0 ± 0.1	0.9-1.1

However, the uncertainty of μ for the SM case is 170% for in the 3000 fb^{-1} case, making impossible to get an evidence of a Higgs boson in the tH process for the same sign muon channel. Even at higher luminosity, the uncertainty of μ in SM case is still very big. In the k_t=-1 model the uncertainty of μ decreases with higher luminosity giving better results. This is caused by the fact that the number of events for the tH signal is greater. For 3000 fb^{-1} the uncertainty on μ is 10%, and it has an upper limit that rounds between 0.9-1.1. In the likelihood scan, the statistical test q gets very high values at μ>1.1. This indicates that for large luminosity this model can be fully ruled out. This can be visualized in the likelihood scan of 3000 fb^{-1}, where the curve is very closed and values of q are very high, giving incompatibility of the model with data.

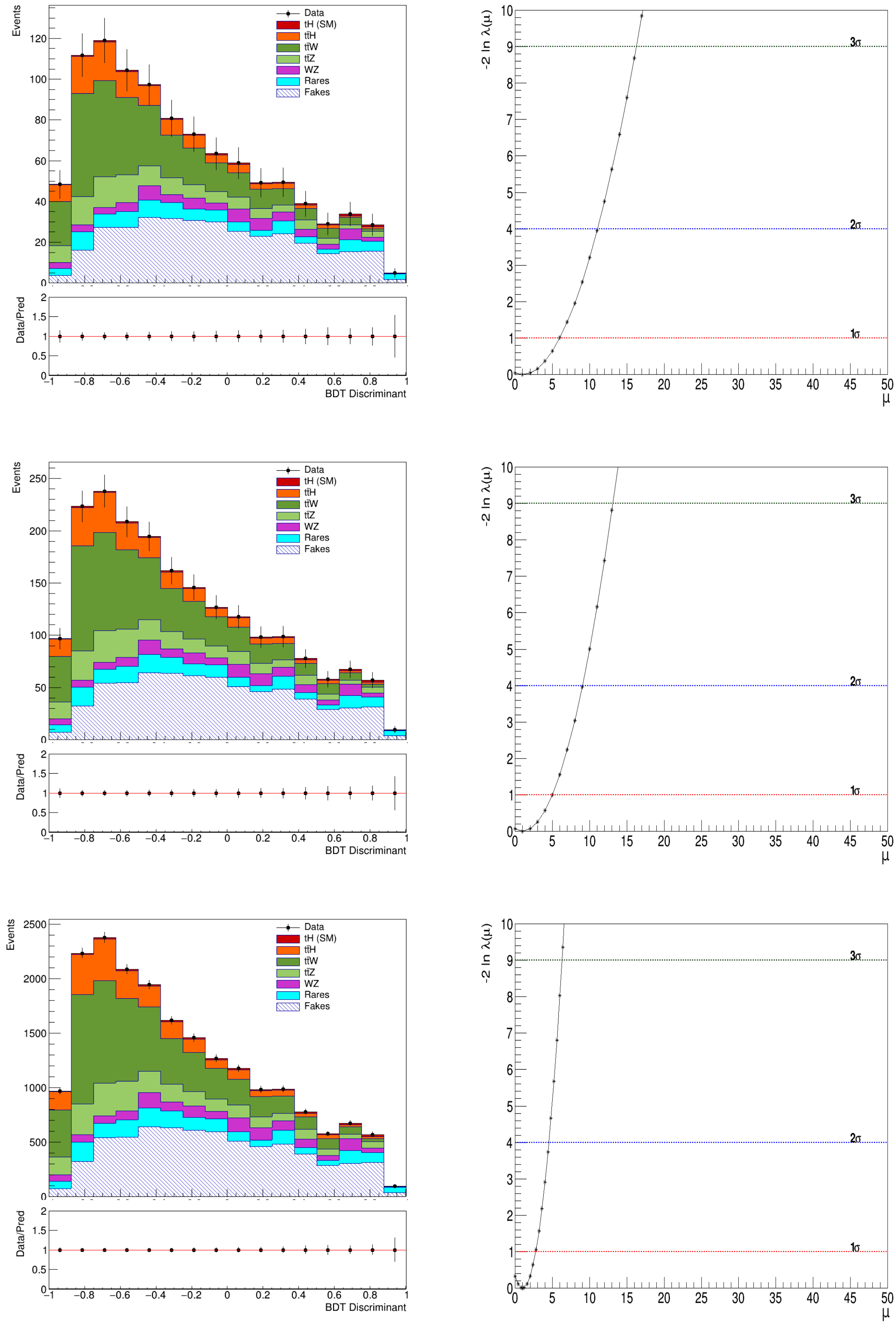

Fig. 4.4 Fit and likelihood scan for 150 fb^{-1}, 300 fb^{-1} and 3000 fb^{-1} in SM

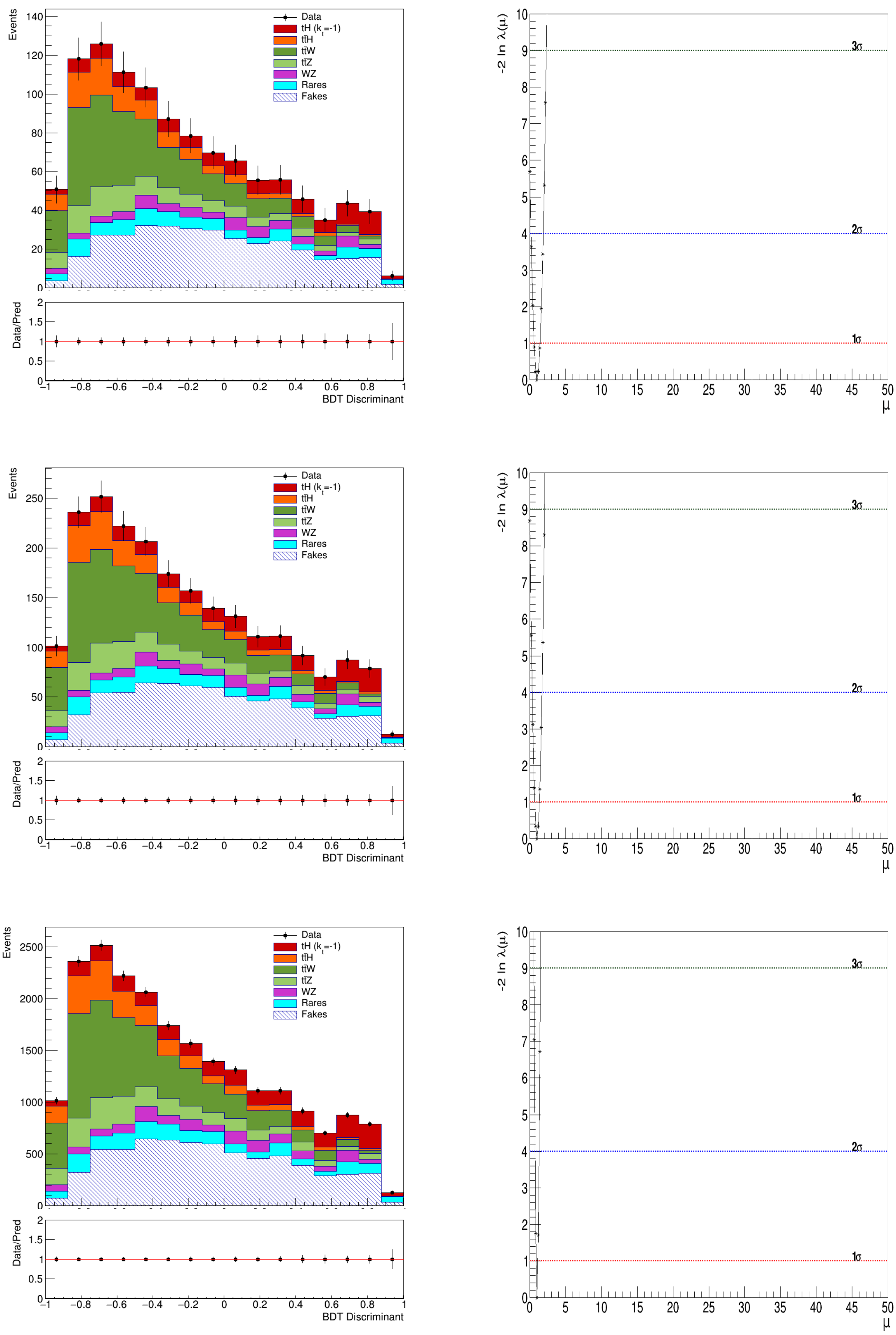

Fig. 4.5 Fit and likelihood scan for 150 fb^{-1}, 300 fb^{-1} and 3000 fb^{-1} in k_t=-1 model.

Chapter 5

Conclusion and outlook

In this work, we explored the sensitivity of the production process of Higgs plus single top. The tH process is an interesting channel in proton-proton collisions in the LHC. This process has not been observed experimentally. Recently CMS published a search for tH production using 35.9 fb^{-1} from Run 2[9]. Using information from this publication, we studied the expected sensitivity using an Asimov data and systematic uncertainties for the final state with same sign pairs of muons.

For an integrated luminosity of 35.9 fb^{-1}, we obtained an expected uncertainty for the tH signal strength μ is around eight times than the value of μ for the SM. In this case, we estimated an upper limit on μ of 17 at 95% confidence level. For the inverted coupling scenario (k_t =-1), the uncertainty after the fit was around 50%, this is due to the larger expected number of signal events.

We also studied the sensitivity for larger integrated luminosity expected in future runs of the LHC. We find that for the SM scenario the expected uncertainty even at the largest integrated luminosity is not enough to observe the signal and only an upper limit on μ is placed at 4.3. In the case of the inverted coupling scenario, a possible signal can be observed with an uncertainty of 10% at 3000 fb^{-1}.

However, these results use only the dimuon channel, the sensitivity can be improved by combining more search channels. The search can include additional channels, such as three lepton in the final state or Higgs decays to a pair of photons. By adding more channels, the number of events increases and can give us better statistics.

References

[1] D. J. Griffiths. "Introduction to elementary particles". *WILEY-VCH Verlag GmbH & Co. KGaA*, 2008.

[2] F. Gross. "Relativistic quantum mechanics and field theory". *WIlEY-VCH Verlag GmbH & Co. KGaA*, 1993.

[3] MissMJ. "Standard Model". URL https://en.wikipedia.org/wiki/Standard_Model#/media/File:Standard_Model_of_Elementary_Particles.svg.

[4] Eric Drexler. "Standard Model". URL https://en.wikipedia.org/wiki/Standard_Model#/media/File:Elementary_particle_interactions_in_the_Standard_Model.png.

[5] Particle Data Group. "Review of particle physics". *Phys. Rev. D*, 98, 030001, Aug 2018. URL https://link.aps.org/doi/10.1103/PhysRevD.98.030001.

[6] CMS collaboration. "Observation of a new boson at a mass of 125 GeV with the CMS experiment at the LHC". *Physics Letters B*, 716(1):30 – 61, 2012. URL https://doi.org/10.1016/j.physletb.2012.08.021.

[7] ATLAS collaboration. "Observation of a new particle in the search for the Standard Model Higgs boson with the ATLAS detector at the LHC". *Physics Letters B*, 716(1): 1 – 29, Sep 2012. URL http://dx.doi.org/10.1016/j.physletb.2012.08.020.

[8] F. Déliot et. al. "Properties of the Top Quark". *Annual Review of Nuclear and Particle Science*, 64:363-381(1), Oct 2014. URL http://dx.doi.org/10.1146/annurev-nucl-102313-025655.

[9] CMS collaboration. "Search for associated production of a higgs boson and a single top quark in proton-proton collisions at $\sqrt{s} = 13$ TeV". *Phys. Rev. D*, 99, 092005, May 2019. URL https://link.aps.org/doi/10.1103/PhysRevD.99.092005.

[10] S. Dawson. "Introduction to electroweak symmetry breaking". (arxiv:hep-ph/9901280), Jan 1999. URL https://arxiv.org/abs/hep-ph/9901280.

[11] P. Langacker. "Introduction to the Standard Model and electroweak physics". *The Dawn of the LHC Era: TASI 2008. Proceedings of the 2008 Theoretical Advanced Study Institute in Elementary Particle Physics*, Aug 2010. URL https://doi.org/10.1142/9789812838360_0001.

[12] ATLAS collaboration. "Search for H $\rightarrow \gamma\gamma$ produced in association with top quarks and constraints on the Yukawa coupling between the top quark and the Higgs boson using data taken at 7 TeV and 8 TeV with the ATLAS detector". *Physics Letters B*, 740:222–242, Jan 2015. URL http://dx.doi.org/10.1016/j.physletb.2014.11.049.

[13] T. Rias. "Higgs boson". URL https://en.wikipedia.org/wiki/Higgs_boson.

[14] LHC Higgs Cross-Section Working Group. "LHC Higgs Cross Section WG Picture Gallery". URL https://twiki.cern.ch/twiki/bin/view/LHCPhysics/LHCHXSWGCrossSectionsFigures.

[15] CMS collaboration. "CMS Physics: Technical design report volume 1: Detector performance and software". Report number: CERN-LHCC-2006-001. 2006. URL http://cds.cern.ch/record/922757.

[16] CMS collaboration. "Search for the th(h$\rightarrow$ b$\bar{\text{b}}$) process in pp collisions at $\sqrt{s} = 13\,\text{TeV}$ and study of higgs boson couplings". Report number: CMS-PAS-HIG-17-016. 2018. URL https://cds.cern.ch/record/2621422.

[17] CERN. "Facts and figures about the LHC ". URL https://home.cern/resources/faqs/facts-and-figures-about-lhc.

[18] CMS collaboration. "CMS detector". URL https://cms.cern/detector.

[19] G. Apollinari et. al. "High-Luminosity Large Hadron Collider (HL-LHC) Technical Design Report V. 0.1". Report number: CERN-2017-007-M. *CERN Yellow Reports: Monographs Archives Vol 4 (2017)*, 2017. URL http://dx.doi.org/10.23731/CYRM-2017-004.

[20] CMS collaboration. "The performance of the CMS muon detector in proton-proton collisions at $\sqrt{s}$= 7 TeV at the LHC". *Journal of Instrumentation*, Volume 8, November 2013. URL http://dx.doi.org/10.1088/1748-0221/8/11/P11002.

[21] A. Hoecker et. al. "TMVA-Toolkit for Multivariate Data Analysis". (arXiv:physics/0703039), 2007. URL https://arxiv.org/abs/physics/0703039.

[22] G. Cowan et. al. "Asymptotic formulae for likelihood-based tests of new physics". *Eur. Phys. J. C 71: 1554*, 71(2), Feb 2011. URL http://dx.doi.org/10.1140/epjc/s10052-011-1554-0.

[23] W. Verkerke & D. Kirkby. "The Roofit Toolkit for Data Modeling". URL http://roofit.sourceforge.net/.